IOP PUBLISHING JOURNAL OF PHYSICS D: APPLIED PHYSICS

J. Phys. D: Appl. Phys. **45** (2012) 175204 (14pp) doi:10.1088/0022-3727/45/17/175204

Hybrid simulation of a dc-enhanced radio-frequency capacitive discharge in hydrogen

P Diomede[1], S Longo[2,3], D J Economou[1] and M Capitelli[2,3]

[1] Plasma Processing Laboratory, Department of Chemical and Biomolecular Engineering, University of Houston, Houston, TX 77204-4004, USA
[2] Dipartimento di Chimica, Universita' degli Studi di Bari, via Orabona 4, 70126 Bari, Italy
[3] CNR-IMIP, Bari Section, via Amendola 122/D, 70126 Bari, Italy

E-mail: padiomede@gmail.com, savino.longo@ba.imip.cnr.it, economou@uh.edu and mario.capitelli@ba.imip.cnr.it

Received 20 December 2011, in final form 5 March 2012
Published 11 April 2012
Online at stacks.iop.org/JPhysD/45/175204

Abstract
A PIC-MCC/fluid hybrid model was employed to study a parallel-plate capacitively coupled radio-frequency discharge in hydrogen, under the application of a dc bias voltage. When a negative dc voltage was applied to one of the electrodes of a continuous wave (cw) plasma, a 'beam' of secondary electrons was formed that struck the substrate counter-electrode at nearly normal incidence. The energy distribution of the electrons striking the substrate extended all the way to $V_{RF} + |V_{dc}|$, the sum of the peak RF voltage and the absolute value of the applied dc bias. Such directional, energetic electrons may be useful for ameliorating charging damage in etching of high aspect ratio nano-features. The vibrational distribution function of molecular hydrogen was calculated self-consistently, and was found to have a characteristic plateau for intermediate values of the vibrational quantum number, v. When a positive dc bias voltage was applied synchronously during a specified time window in the afterglow of a pulsed plasma, the ion energy distributions (IEDs) of positive ions acquired an extra peak at an energy equivalent of the applied dc voltage. The electron energy distribution function was slightly and temporarily heated during the application of the dc bias pulse. The calculated IEDs of H_3^+ and H_2^+ ions in a cw plasma without dc bias were found to be in good agreement with published experimental data.

1. Introduction and literature review

Hydrogen is an essential component in a variety of gas mixtures employed in plasma-enhanced chemical vapour deposition (PECVD). This is mainly due to the high reactivity of H atoms, produced by electron-impact dissociation of molecular hydrogen. For example, a mixture of C_2F_6/H_2 was recently employed to grow graphene films [1]. More classic is the use of CH_4/H_2 or SiH_4/H_2 mixtures for the deposition of diamond-like or amorphous silicon films, respectively [2, 3]. Interesting results have also been obtained in the deposition of germanium from GeH_4/H_2 mixtures [4]. On the other hand, N_2/H_2 plasmas are employed in ashing resists off of low-k dielectric layers [5] and in growing GaN by nitridation of GaAs [6]. Finally, hydrogen diluted mixtures have been used for the deposition of Cu films from organometallic precursors [7]. All these applications will benefit by better understanding the kinetics of hydrogen plasmas.

In particular, the case of pure hydrogen plasma is of relevance in fields as different as space exploration (Jupiter entry), astrophysics, and nuclear fusion (negative ion production for neutral beam injection) [8, 9]. Also, one of the main ions in hydrogen discharges, H_3^+, is an important subject of study in molecular physics [10]. From the variety of plasma reactors used in applications, capacitively coupled radio-frequency (CCRF) plasmas are of particular interest, in view of the large volume of uniform plasma which can be produced. Inevitably, a model of such reactor must include the effect of neutral species on the plasma transport and chemistry. For instance, negative ions are produced

 © 2012 IOP Publishing Ltd Printed in the UK & the USA

by dissociative attachment of vibrationally excited hydrogen molecules [11]. Therefore, the vibrational distribution must be calculated self-consistently with the plasma transport and chemistry including the (generally non-Maxwellian) electron energy distribution function (EEDF).

From the modelling and simulation standpoints, discharges in H_2 or its mixtures with other gases have been studied extensively. Early work focused on the development of plasma chemistry models [12–26]. Although most of these works assumed a spatially uniform plasma, they provided a detailed description of the vibrational distribution by coupling the two-term Boltzmann equation for the EEDF to a 'master' equation for the vibrational distribution function (VDF), and sometimes the population of electronically excited states of molecular species. Such chemical kinetics models played an important role in clarifying the hydrogen plasma chemistry, particularly by providing a quantitative account of the mechanisms of vibrational excitation, molecular dissociation, and ion production, but they were unable to account for the effects of space charge which are necessary in particular for a proper description of CCRF hydrogen discharges. As a result, models were developed coupling species transport and chemical reaction [7, 27–45]. These models varied in the type of formulation (kinetic, fluid or hybrid), the number of spatial dimensions, the degree of self-consistency, and the completeness of the chemical reaction scheme. The works of Longo *et al* [28, 30, 34, 35, 39, 43] analysed the dynamics of charged particles using a 1D in space (3D in velocity) particle-in-cell code with Monte Carlo collisions (PIC-MCC), to follow the transport of electrons and ions subject to collisions with neutral species. The PIC-MCC code was self-consistently coupled to a reaction–diffusion (fluid) equation for the H atoms and the vibrationally excited molecular hydrogen, thus providing a more comprehensive description of low-pressure CCRF hydrogen discharges. Predictions of this hybrid model [35] were compared with both experiments [36, 46] and modelling results [33, 39] by other authors. A 2D PIC-MCC simulation of CCRF hydrogen discharges was presented by Radouane *et al* [29], to study geometry effects in asymmetric reactors (area ratio $\neq 1$), at pressures of $\sim$1 Torr. This work discussed 2D effects and showed comparisons with experimental measurements of the power density and the self-bias voltage. Another 2D PIC-MCC simulation was published by O'Connell *et al* [38] to study ion energy distributions (IEDs) on the electrodes of a hydrogen capacitively coupled plasma (CCP). These last two models neglected the kinetics of neutral species. More recently, Sun *et al* [42] developed a one-dimensional PIC-MCC model to investigate low pressure large-gap hydrogen capacitive discharges driven by combined radio-frequency and pulsed sources focusing on the evolution of the electron energy and density. This model, however, neglected the VDF, and considered only two positive ionic species, namely H^+ and H_2^+, not accounting for H_3^+.

A 1D fluid model including only one ionic species, H_2^+, was developed by Fadlallah *et al* [37] to study the sheath electric field oscillation and the ion kinetics in radio-frequency discharges, finding good agreement with experimental observations, despite the simplified ion kinetics. This model was previously applied to study double layers forming in hydrogen CCPs [36]. A 1D fluid model including electrons, H_3^+, H_2^+, H^+ but no negative ions or the VDF was developed by Lakshmanan and Gill [7] to study Cu thin film deposition from a metalorganic precursor in the pressure range 0.5–10 Torr. The works of Novikova *et al* [31] and Kalache *et al* [32] used a 1D fluid formulation that solved the hydrodynamic equations for charged particles and Poisson's equation for the electric potential. The fluid code was coupled to a kinetic code that assumed a Boltzmann VDF. Despite this last limitation, the model could be used [32] to discuss experimental measurements of H-atom and H^--ion densities. Recently, a kinetic description of the VDF was added to the model and a comparison with the PIC/MCC model by Longo *et al* was performed under controlled conditions [39]. This comparison showed that, to achieve better agreement with the PIC results, the fluid model needed to include an energy equation for ions, especially negative ions, and a calculation of the non-equilibrium EEDF. The work of Salabas *et al* [33] described the dynamics of electrons and positive ions using a two-dimensional self-consistent fluid model with simplified chemistry that neglected vibrational excitation and dissociation (although these were included as loss terms in the electron kinetics module). The simulation results were compared with experimental measurements of the electron density, self-bias voltage, plasma potential and power deposition. The model was also applied to the study of dual frequency hydrogen CCPs [40]. A more detailed chemical kinetics was adopted in [41] where the key role played by the wall recombination of H atoms was shown. Recently, Zhang *et al* [44, 45] used a two-dimensional self-consistent fluid model coupled with the full set of Maxwell equations to investigate the phase-shift effect on the transient behaviour of electrodynamics and power deposition and on the radial uniformity of several plasma characteristics in a hydrogen CCP.

Discharges produced in other than CCP configurations have also been studied in view of their importance for different applications, generally emphasizing ion reactions and H-atom chemistry. For example, Hassouni *et al* [47] developed a 2D multispecies fluid model for a microwave (MW) hydrogen discharge. Agreement with experimental measurements of several quantities was obtained, including H_2 and H temperature versus pressure, H-atom concentration, H_α intensity, and MW field. The relative importance of electron-impact and thermal dissociation channels was determined. Gordiets *et al* [24] studied a travelling wave discharge by a self-consistent model, finding good agreement with experimental results for macroscopic quantities. Méndez *et al* [48] studied a low-pressure hydrogen dc plasma produced in a hollow cathode discharge by means of measurements and a zero-order kinetic model assuming a Maxwellian EEDF and identified the key physicochemical processes determining the plasma composition. Koemtzopoulos *et al* [49] modelled a hydrogen plasma used for deposition of diamond. The EEDF was calculated with a Boltzmann solver based on the two-term approximation. The EEDF in a pure hydrogen plasma was not significantly different from that in a 99%H_2/1%CH_4 plasma used for diamond deposition.

Hydrogen plasmas for the production of negative ions have been studied in an attempt to establish the main production channels and optimize their operation. These models include semi-empirical [50, 51], uniform plasma [8, 52], fluid [53, 54] and particle approaches [55]. Models of discharge mixtures where H_2 is a component have also been developed. Aman-ur-Rehman *et al* [56] employed a fluid model to investigate the effect of pressure on the distribution of H atoms, silylene and silyl radicals in hydrogen/silane discharges. Nienhuis *et al* [57] and Yan and Goedheer [58] studied a H_2/SiH_4 discharge by a fluid model and compared results with experiments of partial pressures of silane, hydrogen, disilane, and the growth rate of amorphous silicon. Kushner [59] modelled $SiH_4/Si_2H_6/H_2$/Ar plasmas by a chemical network with plasma quantities generated in a separate module. Bogaerts and co-workers applied particle models to study the effects of hydrogen addition ($<10\%$) to a RF discharge in Ar [60, 61]. Recently, models of H_2/CH_4 and H_2/C_2H_2 plasmas were developed for studying carbon nanotube deposition [62]. It was found that H_2 has an important effect on the charged particle density and the EEDF. Gordillo-Vázquez *et al* [63] analysed the influence of the excitation frequency of the applied electric field on the EEDF and H-atom concentration near the deposited diamond films (substrate) and in the bulk of $CH_4(\leqslant 5\%)/H/H_2$ plasmas produced in RF and MW discharges through the solution of a stationary homogeneous electron Boltzmann equation and the solution of a kinetic model for the production and loss of H atoms. Hassouni *et al* [64] reviewed modelling issues related to the design of MW cavity for diamond deposition that make use of hydrogen–methane plasmas and to the prediction of active species densities at the growing substrate surface. A two-dimensional fluid model was applied by Salabas *et al* [65] to study plasmas in mixtures of hydrogen and silane. Simulation results yielded the effective electrical power coupled to the plasma, in good agreement with experimental measurements. An analysis of power deposition in a SiH_4/H_2 discharge was performed by Perrin [66] using a uniform model. Hjartarson *et al* [67] and Kimura *et al* [68] both applied a global model to study H_2/Ar discharges. In particular, Hjartason *et al* studied a cylindrical geometry in the 1–100 mTorr pressure range. They found that H_3^+ is the main ion for Ar fraction in hydrogen $<30\%$, and that ArH^+ played a significant role in the H^- chemistry. They confirmed the moderate electronegativity of H_2 discharges (negative ion to electron density ratio $\sim$1 at 100 mTorr). Kimura *et al* studied hydrogen inductively coupled plasmas (ICP) and obtained the H-atom density in fair agreement with actinometric measurements. Lo and Hamaguchi [69] and Donkó *et al* [70] studied pulsed nanosecond high pressure hydrogen microdischarges using PIC/MCC. Under the high-pressure conditions they assumed that the H_2^+ ions were converted effectively to H_3^+ and used a simplified chemistry with only one ionic species (i.e. H_3^+).

Overall, fluid models are most useful at relatively high values of pL (p is pressure and L is characteristic plasma length) for which the computational cost of particle (e.g. PIC-MCC) simulations becomes very high. Kinetic simulations are particularly inefficient in cases involving slow chemical reactions and trace species. However, fluid models cannot provide some important discharge quantities, such as the EEDF. It appears that hybrid models can merge the best qualities of the fluid and kinetic approaches, and are therefore preferable for problems for which the coupling of plasma and neutral species transport and chemistry is important. The hydrogen discharge is such a case.

In this paper, a combined RF/dc CCP in hydrogen was simulated. This configuration is receiving much attention due to the presence of high-energy directional electrons originating by particle bombardment of the dc electrode. Such electrons offer the possibility to tune the plasma density and temperature, or to alleviate charging problems in high aspect ratio features. Radmilovic-Radjenovic and Radjenovic [71] performed a PIC/MCC simulation of an argon CCP source with cylindrical electrodes in order to study the dependence of the breakdown voltage on the product of gas pressure and electrode separation. Simulation results were compared with the experiments of Lisovskiy *et al* [72]. Kawamura *et al* [73, 74] used an analytical model and a PIC/MCC simulation to study the features of RF and dc sheaths and secondary electrons in argon plasmas. Ventzek *et al* [75, 76] used test particle Monte Carlo simulations to analyse the role of ballistic electrons in Ar and CF_4 plasmas. Kushner and co-workers [77] investigated, by means of a two-dimensional hybrid plasma equipment model, the flux of high-energy electrons on the substrate in single and dual frequency dc-augmented CCPs in argon. Wang and co-authors [78, 79] simulated combined RF/dc CCPs in argon by means of particle and hybrid models.

From the experimental point of view, Xu *et al* [80], measured the energy distribution of ballistic electrons in an Ar plasma, while Lisovskiy *et al* [72, 81, 82] studied, by means of experiments and analytical models, the breakdown curves in several gases (e.g. Ar, CF_4, air and N_2). In addition, studies of argon pulsed RF discharges with a dc bias applied in the afterglow have been reported, including particle simulations by Nam *et al* [83] and Diomede *et al* [84], as well as experimental measurements by Xu *et al* [85] and Shin *et al* [86, 87] aimed at obtaining tailored, nearly monoenergetic IED functions.

2. Description of the hybrid model

The one-dimensional in space, three-dimensional in velocity (1D-3v), hydrogen discharge model has been described in detail elsewhere [35, 43]. The hybrid model couples self-consistently a particle-in-cell model with Monte Carlo collisions (PIC-MCC) for charged species (electrons, H^+, H_2^+, H_3^+ and H^- ions), with a reaction–diffusion fluid model for neutrals (14 vibrational levels of the electronic ground state of H_2, and H atoms). Noteworthy features of the PIC-MCC model are the rigorous inclusion of the thermal motion of neutrals in the statistical sampling to determine the ion/neutral collision frequency, and different particle weighting for different species, which allows accurate description of the collision frequency even for species with very low mole fraction.

For the results presented here, the PIC-MCC model was augmented to include anisotropic scattering in electron–H_2

elastic collisions, and more detailed description of secondary electron emission by ion impact on the electrodes. The scattering angles were given by equations (9) and (10) in [88], while the electron velocity components after an electron–H_2 collision were calculated using equation (16) in [89]. The elastic cross section was taken from [90]. Regarding secondary electron emission by ion impact on the electrodes, the speed of the emitted electrons v_e was given by [91]

$$v_e = \left(\frac{2\eta(\varepsilon_{ion} - 2W)}{m_e}\right)^{1/2}, \quad (1)$$

where η is a random number uniformly distributed in [0,1], m_e is the electron mass, ε_{ion} is the bombarding species ionization energy (set equal to 15.4 eV), and W is the work function of the metal electrode (in this case 4.54 eV for tungsten, [92]). The angular distribution and the starting distance from the electrode of the emitted electrons followed equations (5), (6) and (11) of [91]. Under the conditions of this study, the number density of H^+ was an order of magnitude less than that of H_2^+ or H_3^+. Therefore, only the latter two ions were considered to generate secondary electrons by impacting the electrodes. The gas phase and surface chemistry employed in the model can be found in tables 1 and 2 of [35]. Two extra processes were included in this work, namely charge exchange between H^+ and H, and charge exchange between H^- and H. Cross sections for these collisions were taken from [93].

The density of neutral species n_c was obtained by solving the 1D reaction–diffusion equation:

$$\frac{\partial n_c(x,t)}{\partial t} - D_c\frac{\partial^2 n_c(x,t)}{\partial x^2} = \sum_r (\nu'_{rc} - \nu_{rc})k_r \prod_q n_q^{\nu_{rq}} \quad (2)$$

where D_c is the diffusion coefficient of species c, and ν_{rc} is the stoichiometric coefficient of the cth species in the rth elementary reaction. Primed (ν'_{rc}) and un-primed (ν_{rc}) stoichiometric coefficients refer to reaction products and reactants, respectively. For electron-impact reactions, the corresponding rate coefficient k_r was calculated through the EEDF, f_e, as found from the PIC-MCC model,

$$k_r(x,t) = \sqrt{\frac{2}{m_e}}\int_0^\infty \varepsilon f_e(\varepsilon,x,t)\sigma_r(\varepsilon)\,\mathrm{d}\varepsilon \quad (3)$$

where $\sigma_r(\varepsilon)$ is the relevant cross section as a function of electron energy ε. The EEDF was normalized so that the local fraction of electrons with kinetic energy in the range $(\varepsilon, \varepsilon+\mathrm{d}\varepsilon)$ was given by $\varepsilon^{1/2} f_e(\varepsilon, x)\,\mathrm{d}\varepsilon$. Wall reactions included in the fluid model were deactivation of vibrationally excited molecules (reaction probability γ_V) and recombination of H atoms (reaction probability γ_H).

$$H_2(X, v > 0) \xrightarrow{\text{surf.}} H_2(X, v = 0)$$

$$H \xrightarrow{\text{surf.}} \tfrac{1}{2}H_2(X, v). \quad (4)$$

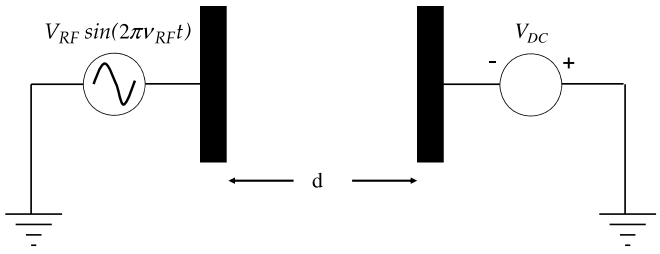

Figure 1. Schematic of a symmetric capacitive discharge driven by an RF power source on one electrode ($x = 0$) and a negative dc source on the other electrode ($x = d$).

The respective boundary conditions were

$$D_{H_2}\frac{\partial n_{H_2(v)}}{\partial \zeta} = \frac{\gamma_V}{4(1-\gamma_V/2)}\cdot\left(\frac{8kT_g}{\pi m_{H_2}}\right)^{1/2} n_{H_2(v)} - p(v)\frac{\gamma_H}{8(1-\gamma_H/2)}\cdot\left(\frac{8kT_g}{\pi m_H}\right)^{1/2} n_H, \qquad v > 0 \quad (5)$$

$$D_H\frac{\partial n_H}{\partial \zeta} = \frac{\gamma_H}{4(1-\gamma_H/2)}\cdot\left(\frac{8kT_g}{\pi m_H}\right)^{1/2} n_H \quad (6)$$

where ζ is the coordinate normal to the surface, directed towards the plasma, k is the Boltzmann constant, T_g is the gas temperature, and $n_{H_2(v=0,\ldots,14)}$ and n_H are the respective neutral species densities in the gas phase close to the surface. Here, $p(v)$ is the probability that the v-level of the VDF is formed as a result of H-atom surface recombination. For the results shown in this paper $p(v) = \delta_{v0}$ i.e. wall recombination resulted in molecules in the $v = 0$ vibrational state. A different choice leads to a slightly more electronegative discharge and a higher population of high vibrational levels as shown in [34].

3. Results and discussion

3.1. dc + RF capacitive discharge

A parallel-plate RF discharge shown schematically in figure 1 was considered. The plates were assumed of large extent (compared with the interelectrode gap, d) so that a one-dimensional treatment was applicable. The left electrode (at $x = 0$) was powered by a continuous wave (cw) RF power supply, while the right electrode (at $x = d$) was powered by a (negative) dc voltage source, also applied continuously. Operating conditions were $d = 6$ cm, pressure $p = 50$ mTorr, gas temperature $T_{gas} = 300$ K, peak RF voltage $V_{RF} = 300$ V, and RF frequency $\nu_{RF} = 13.56$ MHz. The surface reaction probabilities were set to $\gamma_{sec} = 0.1$ for the secondary electron emission by positive ion impact [94], $\gamma_V = 0.02$ for the vibrational deactivation of molecules (within the range of values reported by [13]), and $\gamma_H = 0.1$ for the H-atom recombination (within the range of values reported by [95]).

Figure 2 shows the number densities of electrons and ions as a function of position between the electrodes for different values of the applied dc voltage. The discharge is weakly electronegative, with the negative ion density at the discharge centre somewhat lower than the electron density. The discharge displays the classical structure of electronegative plasmas. Negative ions are 'squeezed' near the discharge

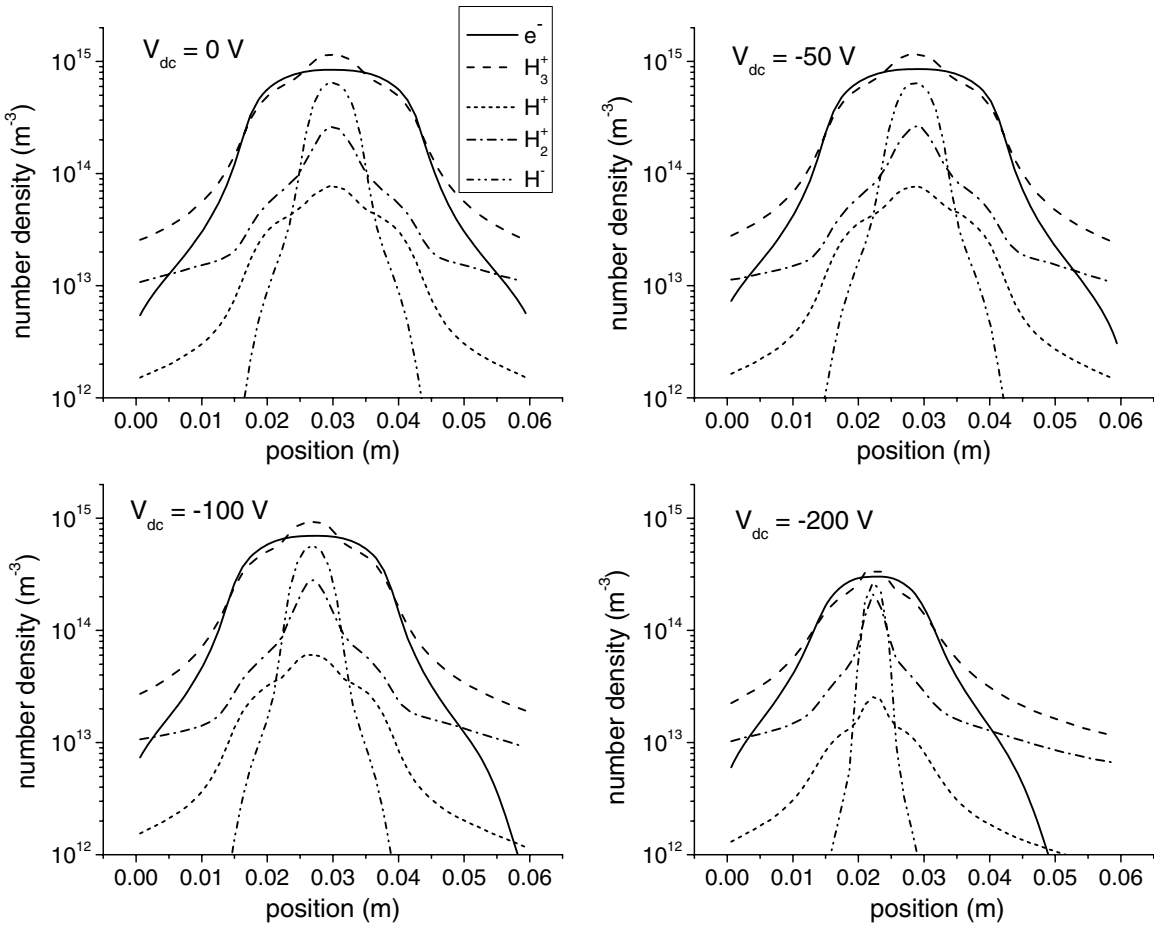

Figure 2. Number densities of electrons and ions across the interelectrode gap, for different values of the applied dc voltage. Other conditions were $d = 6$ cm, $p = 50$ mTorr, $T_{gas} = 300$ K, $V_{RF} = 300$ V, $\nu_{RF} = 13.56$ MHz, $\gamma_{sec} = 0.1$, $\gamma_V = 0.02$, $\gamma_H = 0.1$.

centre where the space (plasma) potential has the most positive value to form an electronegative core. The outer edges of the discharge are electropositive. With no dc bias applied (or with a weak dc bias of −50 V) the discharge is symmetric (or nearly symmetric) around the central plane. Asymmetry develops for more negative values of the dc bias. An electron-free dc sheath is formed next to the dc-biased electrode (at $x = 6$ cm). The sheath thickness increases as the dc voltage becomes more negative, repelling electrons away. As the dc voltage becomes more negative, the positive ion density in the dc sheath decreases slightly, and the negative ion density profile is squeezed further towards the central plane, while the bulk electron density decreases significantly. The decrease in the bulk plasma density at high negative dc bias is due to the reduction of the bulk plasma width, and the corresponding decrease of the volume where ionization occurs. In addition, a reduction of the width of the bulk plasma effectively reduces the positive ion diffusion length (ions from the bulk plasma diffuse to the sheath edge, and then are extracted rapidly by the strong sheath electric field), thus increasing the plasma losses, leading to lower plasma density [73, 74]. The charge densities and the thickness of the RF sheath (next to the electrode at $x = 0$) are mostly unaffected by changes in the dc voltage on the opposite electrode.

In figure 3, the H-atom number density is plotted as a function of position between the electrodes for different values of the applied dc voltage. The atom density corresponds to only 0.1% of the neutral gas density, i.e. a very small degree of molecular dissociation. This is because of the low electron density (less than 10^9 cm^{-3}). Wall consumption of H-atoms by surface recombination leads to a smaller number density near the electrodes. As the dc bias becomes more negative,

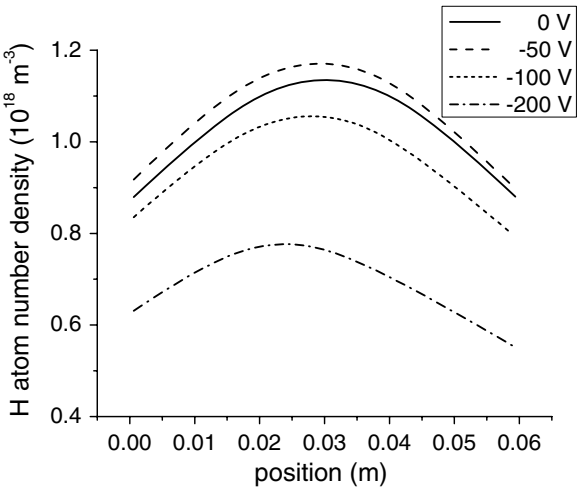

Figure 3. H-atom number density across the interelectrode gap, for different values of the applied dc voltage. Other conditions were the same as in figure 2.

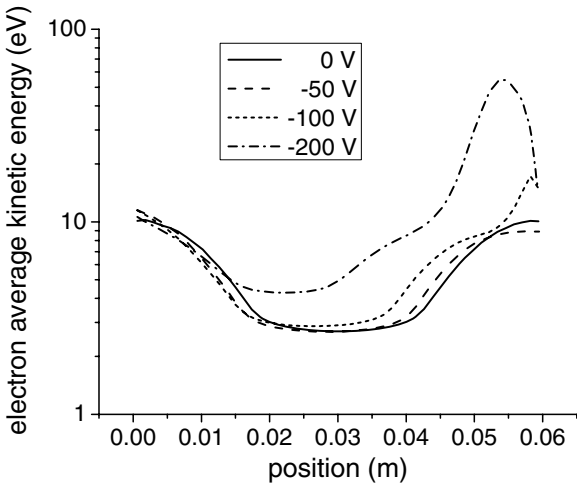

Figure 4. Time-averaged electron kinetic energy across the interelectrode gap, for different values of the applied dc voltage. Other conditions were the same as in figure 2.

the H-atom density first increases, albeit only slightly, and then decreases. The initial slight increase of H-atom density is a reflection of a correspondingly small initial increase in electron density (not discernible in the log scale of figure 2). The decrease in H-atom density at relatively large negative dc bias is due to the reduction of the plasma volume (where H atoms are produced mainly by dissociative excitation of molecular hydrogen), as well as the reduction of electron density.

The spatial profiles of the average electron kinetic energy $\bar{\varepsilon}$ are shown in figure 4, again for different values of the dc voltage. The value of $\bar{\varepsilon}$ generally increases with more negative voltage; slowly as the voltage changes from 0 to -50 V, and then to -100 V, and more rapidly as the voltage becomes -200 V. An exception is the RF sheath, where the average kinetic energy of electrons is nearly independent of the dc voltage. This shows that the RF voltage sustaining the discharge is, at least partially, decoupled from the dc voltage on the counter electrode. This, in turn, implies that there is no appreciable ionization introduced by secondary electrons produced on the dc-biased electrode. Indeed, the maximum ionization cross section (for electron energy $\sim$70 eV) is $\sim 10^{-16}$ cm^2, corresponding to a mean free path of 6 cm, equal to the interelectrode separation, under the present conditions (50 mTorr, 300 K). For a dc voltage of -200 V the average kinetic energy of electrons in the dc sheath, as well as in the bulk plasma, is considerably higher compared with the rest of the cases. This is in part because, at high dc voltages, there is more significant acceleration of secondary electrons in the sheath of the dc electrode, as the inelastic collision mean free path is a decreasing function of energy, for electron energies above $\sim$70 eV [96]. Simulation predictions regarding the behaviour of the dc and RF sheaths, the electron energy, and the plasma density with varying dc voltage are in qualitative agreement with experimental measurements (in nitrogen discharges) [82]. In particular, in figure 2 of [82] it is shown that, for dc voltages smaller than the RF voltage amplitude, the dc sheath width increases with the dc voltage, while the RF sheath width does not change. Moreover,

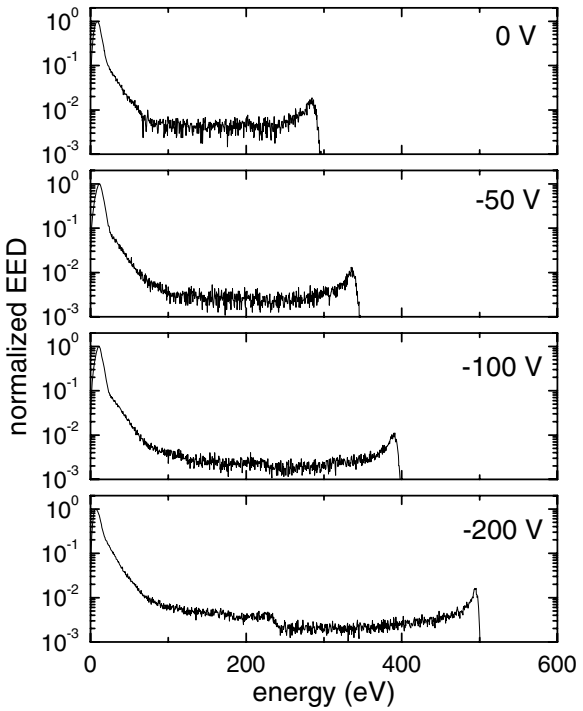

Figure 5. EED at the RF electrode for different values of the applied dc voltage. Other conditions were the same as in figure 2. The distribution functions have been normalized to have a maximum value of unity.

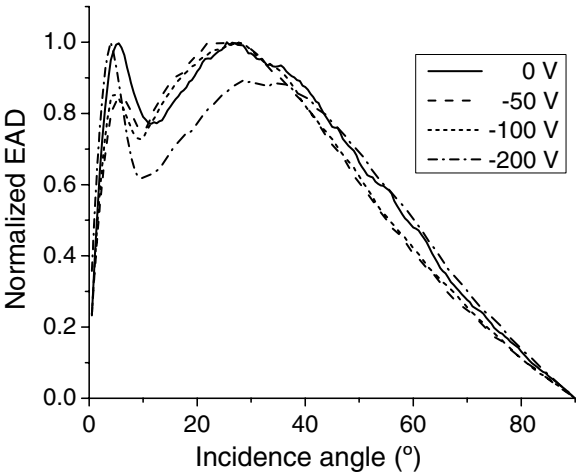

Figure 6. Electron angular distribution at the RF electrode for different values of the applied dc voltage. The incidence angle is with respect to normal on the substrate. Other conditions were the same as in figure 2. The distribution functions have been normalized to have a maximum value of unity.

figure 10 of [82] shows the plasma density decreasing and the bulk electron temperature increasing with the application of a small dc bias to a pure RF discharge. Generally, the same behaviour was predicted in the present study (figures 2 and 4).

The energy and angular distributions of electrons bombarding the RF electrode (at $x = 0$) are shown in figures 5 and 6, respectively, for different values of the applied dc voltage. The electron energy distribution (EED) extends to energies as high as $|V_{dc}| + V_{RF}$, the sum of the absolute value of the dc voltage and the peak RF voltage.

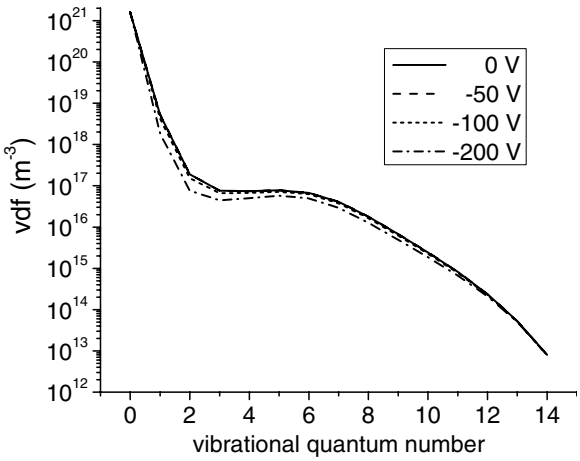

Figure 7. VDF at the position of maximum ion density for different values of the applied dc voltage. Other conditions were the same as in figure 2.

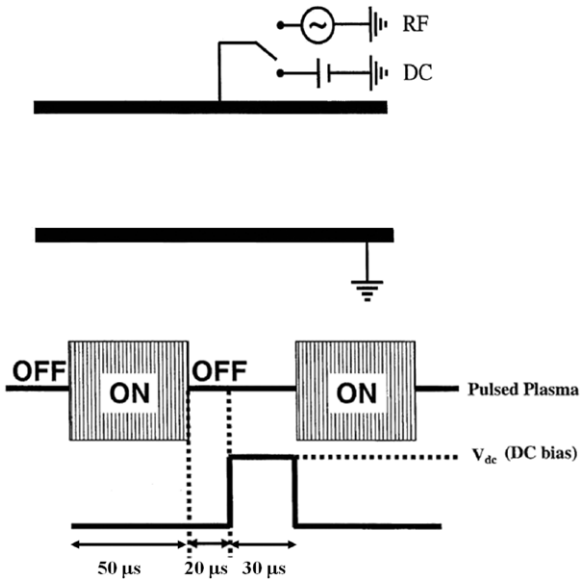

Figure 8. Schematic of a capacitively coupled pulsed plasma reactor. Radio-frequency power (during plasma ON) or a dc bias voltage (during part of the plasma OFF time) was applied to the upper electrode (boundary electrode), while the lower (substrate) electrode was grounded. Time-averaged IEDs were calculated on the substrate electrode.

An approximately bi-Maxwellian distribution is evident for energies up to ∼70 eV. The high-energy electrons originate at the dc-biased electrode by secondary electron emission due to ion bombardment. Such electrons accelerate in the dc sheath and enter the bulk plasma, much like a beam. Under favourable conditions, the electron beam keeps accelerating in the RF sheath as well, yielding electrons with energy $|V_{dc}| + V_{RF}$ close to the maximum of the EED. Rare collisions with gas-phase species or unfavourable timing when entering the RF sheath (e.g. the RF sheath is expanding away from the electrode) can slow down these electrons, resulting in an energy continuum. It should be noted that very high-energy (hundreds of eV) electrons have a relatively small collision cross section. Even when they collide with gas-phase species, such electrons are more likely to be forward scattered forming a beam (sometimes called ballistic electrons [80]). These beam electrons result in a rather sharp peak at low incidence angles superimposed on a wide angular distribution of electrons bombarding the RF electrode (figure 6). The fact that this feature is indeed due to a beam of secondary electrons has been checked by disabling secondary electron emission by ion impact on the electrodes. The beam electrons become slightly more directed as the dc voltage becomes more negative. The low-energy part of the EED (figure 5) consists of bulk thermal electrons, and trapped secondary electrons that have lost their energy in collisions with neutrals [73, 74]. Energetic, directional electrons may be beneficial in ameliorating differential charging (and the ensuing damage) of the bottom and sidewalls of nm-sized high aspect ratio (deep) features, during reactive ion etching in the presence of insulating films [77, 97].

The population of the vibrationally excited states (figure 7) at the position of maximum ion density decreases somewhat with more negative dc bias following the decrease in the electron number density. The plateau in the VDF is because for intermediate values of v, the total production and loss rates of the corresponding vibrational states are almost independent of v [51].

3.2. Pulsed RF discharge with synchronous dc boundary voltage in the afterglow

A pulsed RF discharge with synchronous dc bias in the afterglow was also simulated (figure 8). The plasma-sustaining RF power (applied to the top electrode) was square-wave modulated with a frequency of 10 kHz and a duty cycle of 50%. This resulted in 50 μs of plasma ON (active glow) followed by 50 μs of plasma OFF (afterglow), during each power modulation cycle. There was no dc *self-bias* developed during the active glow due to the symmetry of the discharge. Twenty μs into the afterglow (RF power OFF), a +50 V dc bias voltage (*boundary voltage*) was applied to the top electrode, to raise the plasma potential and expel positive ions out of the plasma. This dc pulse lasted until the end of the afterglow (figure 8, bottom). Other conditions of the hydrogen discharge were as before (d = 6 cm, pressure p = 50 mTorr, gas temperature T_{gas} = 300 K, peak RF voltage V_{RF} = 300 V, and RF frequency ν_{RF} = 13.56 MHz.) Also, as before, γ_{sec} = 0.1, γ_V = 0.02, and γ_H = 0.1.

For this set of operating conditions, a cw RF simulation was first run to reach a periodic steady-state. For 13.56 MHz power, this required ∼1000 RF cycles. The RF voltage was then turned OFF starting the afterglow. Application of the 50 V dc bias voltage commenced 20 μs into the afterglow, until the end of the afterglow. For this time-dependent simulation, scaling of production and loss channels to speed-up convergence of H^- density (applied only for RF periodic steady-state simulations, [98]) was disabled. The number density of the neutral species was updated every 100 PIC-MCC time steps. The plasma ON, plasma OFF, dc ON, dc OFF cycle was repeated ∼120 times to reach a periodic steady-state of the pulsed plasma, the main bottleneck being the slow convergence

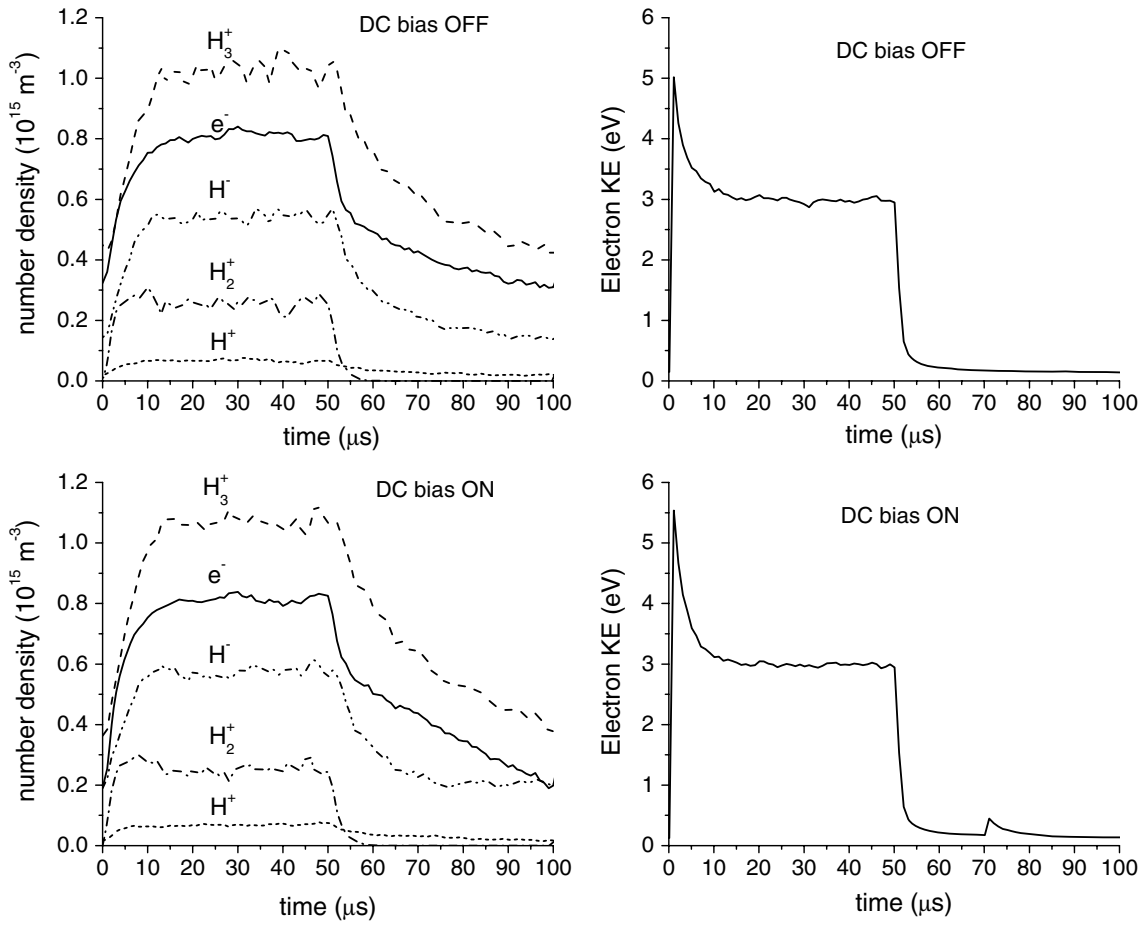

Figure 9. Charged particle number densities and electron average kinetic energy as a function of time at the central plane ($x = 3$ cm) of a pulsed discharge. Top figures were calculated without any dc bias applied. Bottom figures were calculated with +50 V dc bias, applied 20 μs after the start of the afterglow (70 μs after plasma turn-ON) until the end of the afterglow. Other conditions were $d = 6$ cm, $p = 50$ mTorr, $T_{gas} = 300$ K, $V_{RF} = 300$ V (at $\nu_{RF} = 13.56$ MHz) for 50 μs (plasma ON), followed by $V_{RF} = 0$ V for 50 μs (plasma OFF); $\gamma_{sec} = 0.1$, $\gamma_V = 0.02$, $\gamma_H = 0.1$.

of the neutral species and negative ion densities. IEDs were then collected on the substrate (grounded) electrode, similar to the case of an Ar CCP [84].

Figure 9 shows the time evolution of the charged particle number densities and electron kinetic energy at the mid-plane of the discharge ($x = 3$ cm). Results for a pulsed discharge without applying any dc bias in the afterglow are also shown for comparison. As the plasma turns ON at $t = 0\,\mu$s, the charged species number densities increase approaching quasi-steady-state values $\sim$20 μs into the active glow. Under these conditions, the plasma is weakly electronegative and the main positive ion is H_3^+. In the afterglow (commencing at $t = 50\,\mu$s) the charged species densities decay monotonically throughout the afterglow until $t = 100\,\mu$s, when the plasma is turned ON again to repeat the cycle. The time evolution of the charged species densities does not change appreciably when a dc bias is applied in the afterglow (at $t = 70\,\mu$s), except for the electrons that decay a bit faster. The H^- density is slightly higher with the bias ON due to 'squeezing' towards the centre of the negative ions by the rise in the plasma potential. The H_2^+ ions disappear after about 5 μs into the afterglow due to the rapid decay of T_e that quenches production of H_2^+ by ionization of hydrogen molecules, and the fast reaction $H_2^+ + H_2 \rightarrow H_3^+ + H$ that consumes H_2^+.

The electron mean kinetic energy rapidly rises to a peak early in the active glow, only to reach a quasi-steady-state $\sim$10 μs into the active glow. After plasma turn OFF, the electron energy plummets during the first few μs of the afterglow, but decays at a much slower rate later in the afterglow. Later in the afterglow, high threshold energy reactions are quenched. Electron energy decays mainly by diffusion cooling. When a dc bias is applied, temporary heating of the electrons is evident by a weak local peak in electron mean energy starting at 70 μs. This temporary heating is confirmed by examining (figure 10) the time evolution of the electron energy probability function (EEPF). Temporary electron heating (albeit for a short time) results in extension of the tail of the distribution right after the application of the dc bias (right after 70 μs). It is also noted that the EEPF changes from a non-Maxwellian distribution with a high-energy tail during the active glow to a seemingly bi-Maxwellian distribution with a cold tail during the afterglow.

The time evolution during a pulse of the density of the $v = 11$ to $v = 14$ vibrational levels of the ground electronic state of molecular hydrogen, at the discharge centre, is shown in figure 11. The density of the lower vibrational levels is hardly modulated by pulsing the plasma since the time constant of their loss is long compared with the pulse period. The

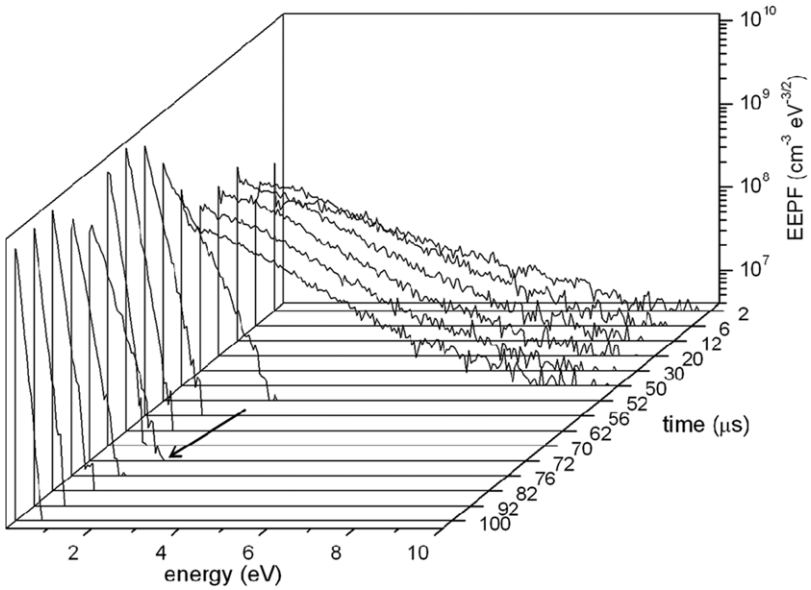

Figure 10. EEPF at the discharge centre for selected times during a pulse, with +50 V dc bias applied 20 μs after the start of the afterglow (70 μs after the plasma is turned ON) until the end of the afterglow. Arrow shows temporarily heated EEPF, upon application of dc bias.

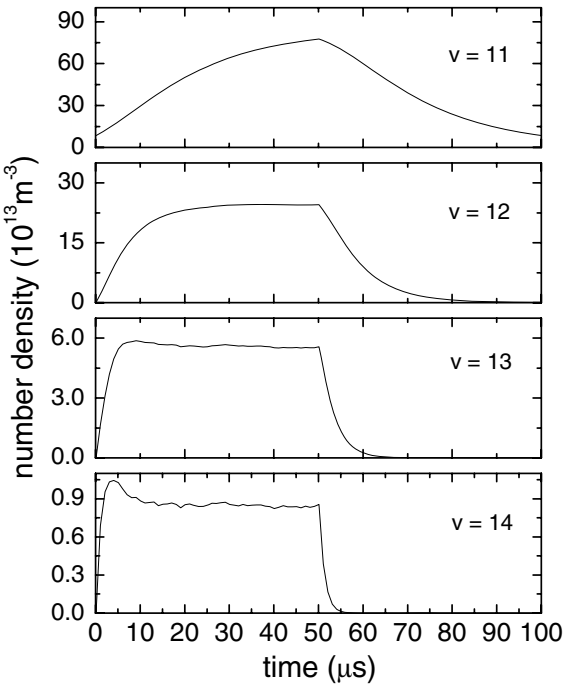

Figure 11. Time evolution of the density of the $v = 11$ to $v = 14$ vibrational levels (of the ground electronic state of molecular hydrogen) at the discharge central plane during a pulse, with +50 V dc bias applied 20 μs after the start of the afterglow (70 μs after the plasma is turned ON) until the end of the afterglow.

high vibrational levels of hydrogen molecules are populated by the so-called EV process which involves an electronic excited state as an intermediate. Since these processes have a high threshold, they are quenched shortly after the plasma is turned OFF. The vibrationally excited states are depopulated mostly by vibrational–translational energy exchange (VT process) involving H_2 molecules and H atoms [34]. The rate coefficients of these processes increase dramatically with the vibrational quantum number. Therefore, the tail of the VDF is quickly quenched after plasma switch-off.

3.3. Ion energy distributions

The (time-averaged over an RF cycle) energy distributions of positive ions bombarding the electrode are shown first for a cw plasma without applied dc bias (figure 12). H^- negative ions are trapped by the ambipolar electric field and cannot reach the walls in a cw plasma. The H_3^+ IED (figure 12(*a*)) shows the classical bimodal structure [99] centred around the average sheath potential (127 V), and a tail towards lower energies due to ion–neutral collisions. The bimodal structure results by ions entering the sheath in different phases of the RF cycle, experiencing a different accelerating potential, depending on when they entered the sheath. The predicted bimodal distribution, with a more intense peak at lower energy, is close to the experimental IED of [38], obtained under similar conditions, reproduced here as figure 12(*b*). The H^+ distribution function (figure 12(*e*)) also has a bimodal structure, but a wider energy spread, compared with H_3^+, due to the lower mass of H^+, yielding a shorter ion transit time. The ion transit time through the sheath can be estimated by $\tau_i \approx 2\bar{s}/\sqrt{2e\bar{V}_s/m_i}$ [99], where $\bar{s}$ and $\bar{V}$ are the time-averaged sheath thickness and sheath potential, respectively, and m_i is the ion mass. This yields an ion transit time of 405 ns, 331 ns, and 234 ns, respectively, for H_3^+, H_2^+ and H^+, while the RF period is $\tau_{RF} = 73.75$ ns. Therefore, the ratio τ_i/τ_{RF} is 5.5, 4.5, and 3.2, respectively for H_3^+, H_2^+ and H^+. The smaller the τ_i/τ_{RF} ratio, the wider the IED. The most structured IED is that of H_2^+ ions (figure 12(*c*)), which exhibits multiple peaks. These peaks can be explained by symmetric charge-exchange collisions [99–101]. In a charge-exchange collision, a fast ion and a thermal gas neutral turn into a fast neutral and a thermal gas ion. If such a collision takes place in the sheath, the newly created ion will experience only a fraction

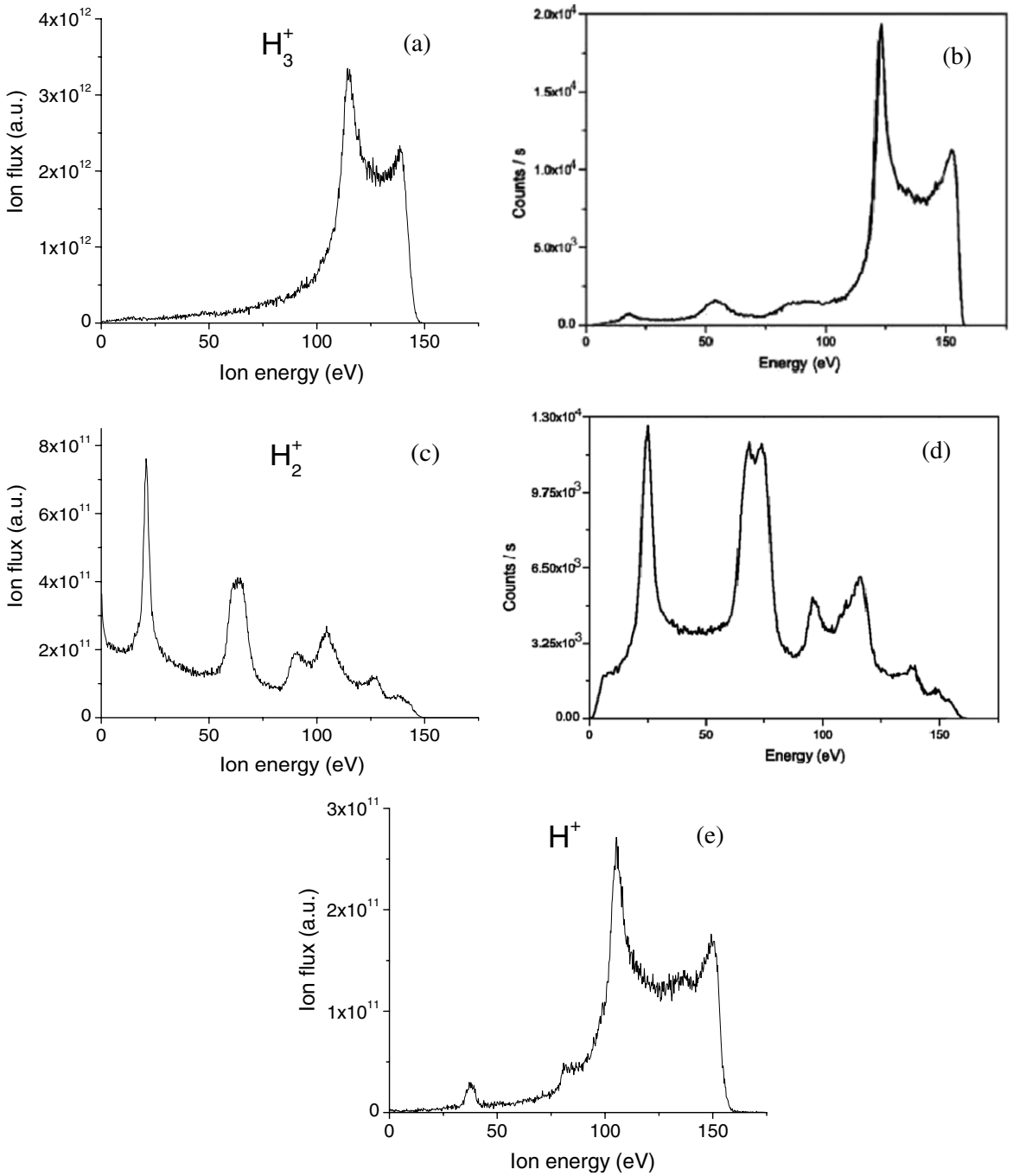

Figure 12. Time-averaged (over an RF cycle) IEDs of H_3^+, H_2^+ and H^+ ions at the grounded electrode (figure 8) of a cw discharge at 50 mTorr. (Other conditions were the same as in figure 2.) (*a*) calculated H_3^+ IED; (*b*) experimental H_3^+ IED [38]; (*c*) calculated H_2^+ IED; (*d*) experimental H_2^+ IED [38]; (*e*) calculated H^+ IED. Measured IEDs in a cw 13.56 MHz hydrogen discharge at 5 Pa (37.5 mTorr), 138 V sheath voltage and 5 cm gap, were reprinted with permission from *Physics of Plasmas*, AIP.

of the sheath voltage. The computed H_2^+ IED is in good agreement with the experimental results of [38], reproduced here as figure 12(*d*). The IED of H_3^+ does not have extra peaks, because these ions cannot suffer symmetric charge-exchange collisions.

Figure 13 shows the effect of lower pressure (20 mTorr) on the IEDs, again for a cw plasma without applied dc bias. It should be noted that, for 20 mTorr, the dominant ion is H_2^+, as confirmed by the experiments of [102]. This is due to the lower rate of conversion of H_2^+ to H_3^+ by the reaction $H_2^+ + H_2 \rightarrow H_3^+ + H$. When compared with 50 mTorr (figure 12), the H_3^+ IED is similar, but the width of the bimodal feature is narrower due to a thicker sheath (smaller electron density and larger electron temperature), making the ion transit time longer. The sheath thickness was about 2.5 cm and 1.8 cm for 20 mTorr and 50 mTorr, respectively. The main bimodal feature of the H^+ IED is also shrunk, again due to the thicker sheath. However, more low-energy peaks appear in the H_2^+ and H^+ distributions, again due to charge-exchange collisions. The peaks on top of the continuum in the low-energy part of the IED are due to ions

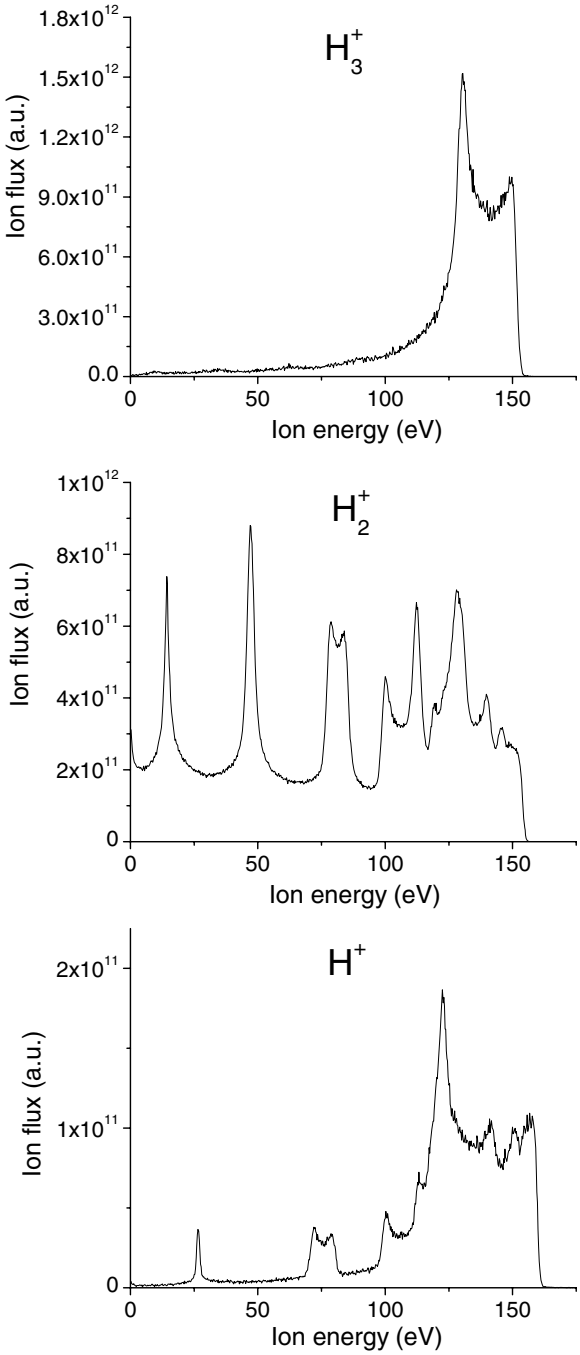

Figure 13. Calculated time-averaged (over an RF cycle) IEDs of H_3^+, H_2^+ and H^+ for the conditions of figure 12 except that the pressure was 20 mTorr.

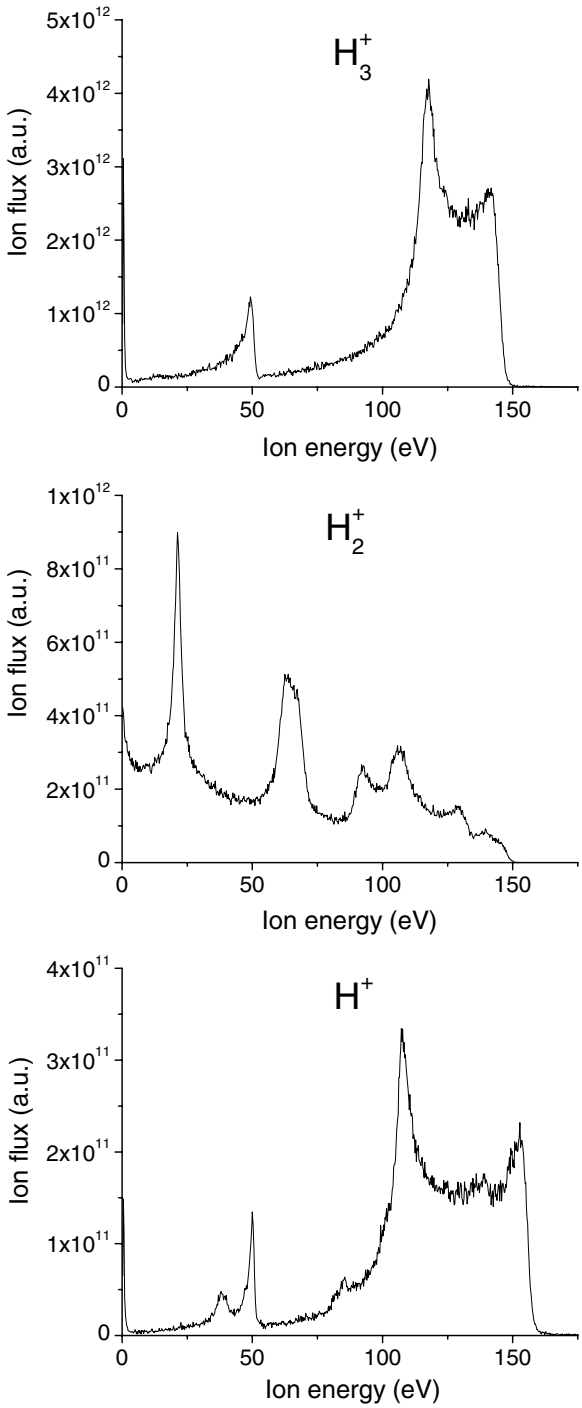

Figure 14. Calculated IEDs of H_3^+, H_2^+ and H^+ at the grounded electrode (figure 8) in a pulsed discharge. The IEDs were time-averaged over a pulse, after the periodic steady-state was achieved. Conditions were 50 mTorr pressure and +50 V dc bias, applied 20 μs after the start of the afterglow, until the end of the afterglow.

created in collisions within the sheath during the time interval when the sheath electric field collapses [99–101].

When a 50 mTorr plasma is pulsed, and a dc bias is applied during part of the afterglow, the IED originating from the power ON fraction of the cycle is retained (figure 14). However, for H^+ and H_3^+, a new peak appears at very low energies, <2 eV, corresponding to ions bombarding the substrate during the afterglow, but before application of the dc bias. After the plasma is turned OFF, the sheath potential collapses within a few microseconds, yielding very low ion bombardment energy during the early afterglow. In each case, the resulting IED has a new distinct peak around 50 eV, corresponding to the dc bias voltage, superimposed on the IED of the cw plasma case. The peak broadening is due to the decay of the plasma potential during the time window over which the dc bias is applied, and also due to ion–neutral collisions. The H_2^+ IED is unaffected by pulsing the plasma or applying a dc bias, since this ion is mostly absent during the afterglow (see figure 9). It should be mentioned that all IEDs in figure 14 were time-averaged over a pulsed plasma cycle.

4. Summary and conclusions

A 1D self-consistent hybrid PIC-MCC/fluid model was employed to study a radio-frequency (RF) parallel-plate capacitively coupled hydrogen discharge under the influence of an externally applied dc bias voltage. Two cases were examined: (a) continuous wave (cw) plasma with a negative dc voltage applied continuously, and (b) pulsed plasma with a positive dc voltage applied synchronously during a specified time window in the afterglow. Under the conditions studied, the hydrogen discharge was moderately electronegative, with the H^- ion density somewhat lower than the electron density. The vibrational distribution function (VDF) of molecular hydrogen exhibited a characteristic plateau for intermediate values of $v = 3$ to $v = 7$. The mole fraction of H atoms, resulting mainly by dissociation of H_2, was very low ($\sim$0.1%) due to the low electron density ($\sim 10^9$ cm^{-3}). At the pressures of 50 mTorr and 20 mTorr, the main positive ions were found to be H_3^+ and H_2^+, respectively.

When a negative dc voltage was applied to a cw plasma (case a), secondary electrons emitted from the dc electrode accelerated in the sheath over that electrode, and entered the bulk plasma. A fraction of these energetic electrons struck the substrate counter-electrode at near normal incidence. The directionality of the electron 'beam' was improved as the dc voltage was made more negative. The electrons striking the substrate had energy as high as ($V_{RF} + |V_{dc}|$), the sum of the peak RF voltage and the absolute value of the dc voltage. Such directional, energetic electrons may alleviate charging problems in plasma processing of high aspect ratio nano-features on the substrate. When the dc voltage was applied, the bulk electron density was slightly increased at first (from no bias to -50 V), only to decrease monotonically for more negative voltages. This was attributed to the reduction of the width of the bulk plasma region under the influence of a sufficiently negative dc bias. The sheath over the RF electrode was almost independent of the value of the dc voltage applied, within the range examined (0 to -200 V). The H_3^+ and H_2^+ ion energy distributions (IEDs) on the substrate electrode were found to be in good agreement with published experimental data for a cw plasma without applied dc bias.

When a positive dc voltage was applied synchronously in part of the afterglow of a pulsed plasma (case b), the time evolution of the electron, positive ion and negative ion densities was influenced only slightly. The electron energy probability function (EEPF) was temporarily heated at the moment of the application of the dc bias, resulting in a slight and temporary increase in the average electron kinetic energy. The density of the vibrational states with high v ($v = 11$ to $v = 14$) was deeply modulated under the 10 kHz (50% duty cycle) pulsed plasma frequency. In contrast to H_3^+, the IEDs of H_2^+ and H^+ were decorated with multiple peaks due to symmetric charge-exchange collisions with H_2 molecules and H atoms, respectively. A distinct peak at the value of the applied bias voltage appeared in the IEDs of H_3^+ and H^+ compared with the case of no applied bias. The IED of H_2^+ was the same under cw or pulsed plasma conditions, since the H_2^+ ion was quickly eliminated in the early afterglow by converting to H_3^+.

The present model does not account for secondary electrons emitted by electron impact on the electrodes. This can be important, especially on electrodes with large value of the corresponding emission coefficient [80], and it is the subject of continuing investigations.

Acknowledgments

PD and DJE are grateful to the Department of Energy, Office of Fusion Energy Science, contract DE-SC0001939, the National Science Foundation grant CBET 0903426, and the Department of Energy grant DE-SC0000881 for financial support of this work. SL and MC acknowledge partial support from MIUR grant ex-60% 2010 Universita' di Bari.

References

[1] Hiramatsu M, Shiji K, Amano H and Hori M 2004 *Appl. Phys. Lett.* **84** 4708
[2] May P W, Harvey J N, Smith J A and Mankelevich Yu A 2006 *J. Appl. Phys.* **99** 104907
[3] Park Y-B, Li X, Rhee S-W and Park D-W 1999 *J. Phys. D: Appl. Phys.* **32** 1955
[4] Sakata T, Makihara K, Deki H, Higashi S and Miyazaki S 2007 *Mater. Sci. Forum* **561–565** 1209
[5] Morikawa Y *et al* 2001 *J. Vac. Sci. Technol.* A **19** 1747
[6] Losurdo M *et al* 1999 *J. Vac. Sci. Technol.* A **17** 2194
[7] Lakshmanan S K and Gill W N 1999 *Thin Solid Films* **338** 24
[8] Capitelli M *et al* 2006 *Nucl. Fusion* **46** S260–74
[9] Franzen P, Schiesko L, Fröschle M, Wünderlich D, Fantz U and the NNBI Team 2011 *Plasma Phys. Control. Fusion* **53** 115006
[10] Oka K 1983 The H_3^+ ion *Molecular Ions, Spectroscopy. Structure and Chemistry* ed T A Miller and V E Bondybey (Amsterdam: North Holland)
[11] Bacal M 2006 *Nucl. Fusion* **46** S250–9
[12] Cacciatore M, Capitelli M and Dilonardo M 1978 *Chem. Phys.* **34** 193
[13] Gorse C, Capitelli M, Bretagne J and Bacal M 1985 *Chem. Phys.* **93** 1
[14] Capitelli M (ed) 1986 *Nonequilibrium Vibrational Kinetics* (*Topics in Current Physics*) (Berlin: Springer)
[15] Gorse C, Capitelli M, Bacal M, Bretagne J and Laganà A 1987 *Chem. Phys.* **117** 177
[16] Loureiro J and Ferreira C M 1989 *J. Phys. D: Appl. Phys.* **22** 1680
[17] Celiberto R, Capitelli M and Cacciatore M 1990 *Chem. Phys.* **140** 209
[18] Gorse C, Celiberto R, Cacciatore M, Laganà A and Capitelli M 1992 *Chem. Phys.* **161** 211
[19] Garscadden A and Napgal R 1995 *Plasma Sources Sci. Technol.* **4** 268
[20] Amorim J, Loureiro J, Baravian G and Touzeau M 1997 *J. Appl. Phys.* **82** 2795
[21] Gordiets B F, Ferreira C M, Pinheiro M J and Ricard A 1998 *Plasma Sources Sci. Technol.* **7** 363
[22] Loureiro J and Amorim J 1998 *Chem. Phys.* **232** 141
[23] Hassouni K, Gicquel A, Capitelli M and Loureiro J 1999 *Plasma Sources Sci. Technol.* **8** 494
[24] Gordiets B, Pinheiro M, Tatarova E, Dias F M, Ferreira C M and Ricard A 2000 *Plasma Sources Sci. Technol.* **9** 295
[25] Amorim J, Loureiro J and Schram D 2001 *Chem. Phys. Lett.* **346** 443

[26] Capitelli M, Celiberto R, Esposito F, Laricchiuta A, Hassouni K and Longo S 2002 *Plasma Sources Sci. Technol.* **11** 7

[27] Boeuf J P and Pitchford L C 1995 SIGLO-RF, Kinema Software, Monument, CO (http://www.siglo-kinema.com/siglo-rf.htm)

[28] Longo S and Boyd I D 1998 *Chem. Phys.* **238** 445

[29] Radouane K, Despax B, Yousfi M, Couderc J P, Klusmann E, Meyer H, Schulz R and Schulze J 2001 *J. Appl. Phys.* **90** 4346

[30] Longo S and Milella A 2001 *Chem. Phys.* **274** 219

[31] Novikova T, Kalache B, Bulkin P, Hassouni K, Morscheidt W and Roca i Cabarrocas P 2003 *J. Appl. Phys.* **93** 3198

[32] Kalache B, Novikova T, Fontcuberta i Morral A, Roca i Cabarrocas P, Morscheidt W and Hassouni K 2004 *J. Phys. D: Appl. Phys.* **37** 1765

[33] Salabas A, Marques L, Jolly J, Gousset G and Alves L L 2004 *J. Appl. Phys.* **95** 4605

[34] Diomede P, Longo S and Capitelli M 2005 *Eur. Phys. J.* D **33** 243

[35] Diomede P, Capitelli M and Longo S 2005 *Plasma Sources Sci. Technol.* **14** 459

[36] Leroy O, Stratil P, Perrin J, Jolly J and Belenguer P 1995 *J. Phys. D: Appl. Phys.* **28** 500

[37] Fadlallah M, Booth J-P, Derouard J, Sadeghi N and Belenguer P 1996 *J. Appl. Phys.* **79** 8976

[38] O'Connell D, Zorat R, Ellingboe A R and Turner M M 2007 *Phys. Plasmas* **14** 103510

[39] Diomede P, Michau A, Redolfi M, Morscheidt W, Hassouni K, Longo S and Capitelli M 2008 *Phys. Plasmas* **15** 103505

[40] Salabas A and Brinkmann R P 2005 *Plasma Sources Sci. Technol.* **14** S53

[41] Marques L, Jolly J and Alves L L 2007 *J. Appl. Phys.* **102** 063305

[42] Sun J, Li X, Sang C, Jiang W, Zhang P and Wang D 2010 *Phys. Plasmas* **17** 103505

[43] Longo S and Diomede P 2009 *Plasma Process. Polym.* **6** 370

[44] Zhang Y-R, Xu X, Bogaerts A and Wang Y-N 2012 *J. Phys. D: Appl. Phys.* **45** 015202

[45] Zhang Y-R, Xu X, Bogaerts A and Wang Y-N 2012 *J. Phys. D: Appl. Phys.* **45** 015203

[46] Jolly J and Booth J-P 2005 *J. Appl. Phys.* **97** 103305

[47] Hassouni K, Grotjohn T A and Gicquel A 1999 *J. Appl. Phys.* **86** 134

[48] Méndez I, Gordillo-Vázquez F J, Herrero V J and Tanarro I 2006 *J. Phys. Chem.* A **110** 6060

[49] Koemtzopoulos C R, Economou D J and Pollard R 1993 *Diamond Relat. Mater.* **2** 25–35

[50] Hiskes J R and Karo A M 1989 *Appl. Phys. Lett.* **54** 508

[51] Mosbach T 2005 *Plasma Sources Sci. Technol.* **14** 610

[52] Capitelli M and Gorse C 2005 *IEEE Trans. Plasma Sci.* **33** 1832

[53] Boeuf J P, Hagelaar G J M, Sarrailh P, Fubiani G and Kohen N 2011 *Plasma Sources Sci. Technol.* **20** 015002

[54] Paunska Ts, Shivarova A, Tarnev Kh and Tsankov Ts 2011 *Phys. Plasmas* **18** 023503

[55] Taccogna F, Minelli P, Diomede P, Longo S, Capitelli M and Schneider R 2011 *Plasma Sources Sci. Technol.* **20** 024009

[56] Aman-ur-Rehman, Kwon H C, Park W T and Lee J K 2011 *Phys. Plasmas* **18** 093502

[57] Nienhuis G J, Goedheer W J, Hamers E A G, van Sark W G J H M and Bezemer J 1997 *J. Appl. Phys.* **82** 2060

[58] Yan M and Goedheer W J 1999 *IEEE Trans. Plasma Sci.* **27** 1399

[59] Kushner M J 1988 *J. Appl. Phys.* **63** 2532

[60] Neyts E, Yan M, Bogaerts A and Gijbels R 2003 *Nucl. Instrum. Methods Phys. Res.* B **202** 300

[61] Neyts E, Yan M, Bogaerts A and Gijbels R 2003 *J. Appl. Phys.* **93** 5025

[62] Mao M and Bogaerts A 2010 *J. Phys. D: Appl. Phys.* **43** 205201

[63] Gordillo-Vázquez F J, Gómez-Aleixandre C and Albella J M 2001 *Plasma Sources Sci. Technol.* **10** 99

[64] Hassouni K, Silva F and Gicquel A 2010 *J. Phys. D: Appl. Phys.* **43** 153001

[65] Salabas A, Gousset G and Alves L L 2002 *Plasma Sources Sci. Technol.* **11** 448

[66] Perrin J 1993 *J. Phys. D: Appl. Phys.* **26** 1662

[67] Hjartarson A T, Thorsteinsson E G and Gudmundsson J T 2010 *Plasma Sources Sci. Technol.* **19** 065008

[68] Kimura T and Kasugai H 2010 *J. Appl. Phys.* **107** 083308

[69] Lo C-W and Hamaguchi S 2011 *J. Phys. D: Appl. Phys.* **44** 375201

[70] Donkó Z, Schulze J, Muller S and Czarnetzki U 2011 *Appl. Phys. Lett.* **98** 251502

[71] Radmilovic-Radjenovic M and Radjenovic B 2006 *Plasma Sources Sci. Technol.* **15** 1

[72] Lisovskiy V A and Yegorenkov V D 1994 *J. Phys. D: Appl. Phys.* **27** 2340

[73] Kawamura E, Lieberman M A, Lichtenberg A J and Hudson E A 2007 *J. Vac. Sci. Technol.* A **25** 1456

[74] Kawamura E, Lichtenberg A J and Lieberman M A 2008 *Plasma Sources Sci. Technol.* **17** 045002

[75] Denpoh K and Ventzek P L G 2008 *J. Vac. Sci. Technol.* A **26** 1415

[76] Ventzek P L G and Denpoh K 2009 *J. Vac. Sci. Technol.* A **27** 287

[77] Wang M and Kushner M J 2010 *J. Appl. Phys.* **107** 023308

[78] Jiang W, Xu X, Dai Z-L and Wang Y-N 2008 *Phys. Plasmas* **15** 033502

[79] Wang S, Xu X and Wang Y 2012 *Plasma Sci. Technol.* **14** 32

[80] Xu L, Chen L, Funk M, Ranjan A, Hummel M, Bravenec R, Sundararajan R, Economou D J and Donnelly V M 2008 *Appl. Phys. Lett.* **93** 261502

[81] Lisovskiy V A, Kharchenko N D and Yegorenkov V D 2010 *J. Phys. D: Appl. Phys.* **43** 425202

[82] Lisovskiy V A, Kharchenko N D and Yegorenkov V D 2008 *J. Phys. D: Appl. Phys.* **41** 125207

[83] Nam S K, Economou D J and Donnelly V M 2007 *Plasma Sources Sci. Technol.* **16** 90

[84] Diomede P, Economou D J and Donnelly V M 2011 *J. Appl. Phys.* **109** 083302

[85] Xu L, Economou D J, Donnelly V M and Ruchhoeft P 2005 *Appl. Phys. Lett.* **87** 041502

[86] Shin H, Zhu W, Xu L, Economou D J and Donnelly V M 2011 *Plasma Sources Sci. Technol.* **20** 055001

[87] Shin H, Zhu W, Economou D J and Donnelly V M 2012 *J. Vac. Sci. Technol.* A **30** 021306

[88] Vahedi V and Surendra M 1995 *Comput. Phys. Commun.* **87** 179–98

[89] Longo S 2006 *Plasma Sources Sci. Technol.* **15** S181

[90] http://consult.cern.ch/writeup/magboltz/

[91] Krimke R and Urbassek H M 1996 *J. Phys. D: Appl. Phys.* **29** 378–87

[92] Lieberman M A and Lichtenberg A J 2005 *Principles of Plasma Discharges and Materials Processing* 2nd edn (Hoboken, NJ: Wiley)

[93] Eletskii A V 1997 Elementary processes in gases and plasmas *Handbook of Physical Quantities* ed I S Grigoriev and E Z Meilikhov (Boca Raton, FL: CRC Press) pp 489–514, and Table 18.11, p 498

[94] Chapman B 1980 *Glow Discharge Processes* (New York: Wiley)

[95] Kae-Nune P, Perrin J, Jolly J and Guillon J 1996 *Surf. Sci.* **360** L495–8

[96] Christophorou L G (ed)1984 *Electron–Molecule Interactions and Their Applications* vol 2 (Orlando, FL: Academic) p 192
[97] Wang M and Kushner M J 2010 *J. Appl. Phys.* **107** 023309
[98] Diomede P, Longo S and Capitelli M 2006 *Phys. Plasmas* **13** 113505
[99] Kawamura E, Vahedi V, Lieberman M A and Birdsall C K 1999 *Plasma Sources Sci. Technol.* **8** R45
[100] Wild C and Koidl P 1989 *Appl. Phys. Lett.* **54** 505
[101] Wild C and Koidl P 1991 *J. Appl. Phys.* **69** 2909
[102] Nunomura S and Kondo M 2007 *J. Appl. Phys.* **102** 093306